Approximate method for gap soliton propagation in nonuniform Bragg gratings

Neil G. R. Broderick* and C. Martijn de Sterke
School of Physics, University of Sydney, Sydney 2006, Australia
and Australian Photonics Cooperative Research Centre, Australian Technology Park, Eveleigh, 1430, Australia
(Received 10 July 1998)

An effective particle picture developed earlier for gap soliton propagation in piecewise uniform gratings is extended to treat gratings that vary gradually. In particular, we consider gratings in which the strength or the Bragg frequency varies linearly with position. We use this to analyze propagation in more complicated structures corresponding to localized grating defects, and gradual interfaces between two different gratings. [S1063-651X(98)07312-7]

PACS number(s): 42.65.Tg, 42.65.Pc, 42.70.Qs

I. INTRODUCTION

Earlier this year Taverner and co-workers reported the first observations of gap soliton generation in a Bragg grating at frequencies within the photonic band gap [1,2]. These experiments compliment those of Eggleton and co-workers [3–5], who examined propagation through Bragg gratings at frequencies outside the band gap, where the grating is transmissive but highly dispersive. In the experiments by Taverner and co-workers [1,2] and in the most recent ones by Eggleton *et al.* [5], nonuniform gratings were used to optimize the coupling of the light into the grating. Furthermore both sets of experiments were performed in relatively short gratings (8 cm in Refs. [1,2], 6 cm in Ref. [5]). Thus, in these experiments, pure soliton propagation effects are difficult to distinguish from effects due to soliton formation. However, in future experiments, gap soliton propagation over longer lengths is likely to be studied; note that currently the maximum available length for a fiber Bragg grating is roughly 1 m [6].

In the experiments of Taverner and co-workers the grating length was 8 cm, as this was the maximum length over which uniformity of the Bragg frequency could be assured. In writing longer fiber Bragg gratings this uniformity decreases due to random refractive index fluctuations, as well as to temperature drifts during the writing process. Thus if gap soliton propagation over long distances is to be experimentally observed, then gap solitons must be stable to small perturbations.

Light propagation in nonlinear Bragg gratings is usually described using the nonlinear coupled mode equations (NLCME's). These apply to both $\chi^{(3)}$ materials [7–9] and to $\chi^{(2)}$ materials in the cascading limit [10]. Gap solitons are solitary wave solutions to the NLCME [11–13], and can propagate at any speed between zero and the speed of light in the uniform medium. Much of the interest in gap solitons has focused on those solutions whose frequency content is inside the grating's band gap [2,8], where, in the linear regime, light cannot propagate. However, gap solitons with frequencies outside the band gap, grating solitons, where the grating is highly dispersive, have also attracted considerable attention [3–5].

Predicting the behavior of gap solitons in the presence of small perturbations requires some analytic approximation to the NLCME's, since they cannot be solved exactly. Similarly, perturbations to the nonlinear Schrödinger equation (NLSE) are also rarely tractable. Therefore, a wide range of approximate methods has been developed to deal with soliton propagation (for example in Ref. [14]). Most of these rely on the fact that if the field can initially be described as a soliton, then it remains a soliton. As solitons are characterized by a small number of real parameters, the perturbations lead to a set of ordinary differential equations for the soliton parameters [14]. This is a considerable simplification compared to the full problem, which requires solving a nonlinear partial differential equation. Such methods can be described as effective particle pictures (EPP's), since they represent the continuous field distribution as a point particle with a limited number of degrees of freedom.

The key difference between the NLSE and NLCME's is that the NLSE is integrable [15] whereas NLCME's are not. This suggests that NLSE solitons are more robust than gap solitons, and hence that an EPP would be more accurate in that case. However, previously, gap soliton propagation in the presence of uniform gain and loss was succesfully treated using an EPP [16,17], and we ourselves examined gap soliton propagation across abrupt interfaces using a similar technique [18]. Hence it is natural to apply the EPP to more general perturbations. The EPP we developed is similar to one used by Aceves, Newell, and Moloney [14] to treat NLSE soliton propagation across an interface. The method was also used by Capobianco *et al.* to treat propagation between two quadratically nonlinear materials [19]. In this paper we extend our earlier work [18] to show that the EPP works for nonuniform gratings whose parameters change continuously.

The outline of this paper is as follows: In Sec. II we outline the EPP we derived previously, and discuss some of its more general features. We then use the EPP in Sec. III to treat gap soliton propagation in simple structures, before combining these structures to treat more complicated perturbations in Secs. IV and V.

*Present address: Optoelectronics Research Center, University of Southampton, Southampton, U.K.

II. EFFECTIVE PARTICLE APPROACH

Light propagation in Bragg gratings is usually described by the nonlinear coupled mode equations [8]. However, in the presence of perturbations we need to modify these accordingly. Using a complex matrix V_{ij} to describe the perturbations, the modified coupled mode equations are written as [18]

$$i\frac{\partial f_+}{\partial x}+\frac{i}{v_g}\frac{\partial f_+}{\partial t}+\kappa f_-+2\Gamma_x|f_-|^2f_+ +\Gamma_s|f_+|^2f_++V_{11}(x)f_++V_{12}(x)f_-=0, \tag{1a}$$

$$-i\frac{\partial f_-}{\partial x}+\frac{i}{v_g}\frac{\partial f_-}{\partial t}+\kappa f_++2\Gamma_x|f_+|^2f_- +\Gamma_s|f_-|^2f_-+V_{21}(x)f_++V_{22}(x)f_-=0, \tag{1b}$$

where $f_\pm$ are the slowly varying envelopes of the forward and backward propagating waves at the Bragg frequency ω_0. The group velocity v_g, which determines the speed of the fields in the absence of a grating, is set equal to unity by a rescaling of the time t. Parameter κ describes the grating strength, and Γ_s and Γ_x determine the strength of the self- and cross-phase modulations, respectively. In optical fibers with a $\chi^{(3)}$ nonlinearity (and most other materials) $\Gamma_s=\Gamma_x$. However the NLCME's also describe light propagation through a $\chi^{(2)}$ material, and in that case the value of Γ_s/Γ_x is determined by the frequencies involved and can take almost any value [20].

Since in Eqs. (1) we assumed that the perturbations are proportional to the fields, the matrix V is unable to represent the effects of a driving term. However, most other perturbations can be represented in this manner. We note that when the perturbation is nonlinear, the elements of V depend on the envelopes themselves. We restrict our analysis to a Hermitian V, as this represents a lossless medium. The effects of gain and loss have been treated previously [16,17], and our analysis reproduces their results in the appropriate limit.

In the absence of any perturbations ($V_{ij}=0$), the NLCME's possess the following gap solitons solutions found by Aceves and Wabnitz [11]:

$$f_\pm(x,t)=\pm\alpha\sqrt{\frac{\kappa}{2\Gamma_x}}\left(\frac{1\pm\chi}{1\mp\chi}\right)^{1/4}\sin\rho \times\operatorname{sech}(\theta\mp i\rho/2)e^{i(\sigma+\eta)}, \tag{2}$$

where the nonlinearity was taken to be positive. Further,

$$\theta=\gamma\kappa\sin(\rho)(x-x_0-\chi t), \tag{3}$$

$$\sigma=\gamma\kappa\cos(\rho)(\chi x-t-t_0), \tag{4}$$

$$\alpha=\left(1+\frac{\Gamma_s}{2\Gamma_x}\frac{1+\chi^2}{1-\chi^2}\right)^{-1/2}, \tag{5}$$

$$e^{i\eta}=\left(-\frac{e^{2\theta}+e^{\mp i\rho}}{e^{2\theta}+e^{\pm i\rho}}\right)^{2\Gamma_s v/[2\Gamma_x(1-v^2)+\Gamma_s(1+v^2)]}, \tag{6}$$

where $\gamma=1/\sqrt{1-\chi^2}$ is the Lorentz factor. Note that if $\Gamma_s=\Gamma_x$, then $\alpha^2\to\frac{2}{3}$ as $\chi\to0$. Also, $\alpha\to0$ as $\chi\to\pm1$.

The gap soliton velocity is given by χv_g, where $\chi\in[-1,1]$. The center frequency is given by $\Omega=\gamma\kappa\cos(\rho)$, and ρ is restricted to the range $[0,\pi]$. Note that the center frequency of the gap soliton can be arbitrarily far from the Bragg frequency ω_0. For $|\Omega|<\kappa$ the center frequency is within the grating's band gap [8].

For the application of the EPP it is important that the solutions depend on four parameters t_0, x_0, ρ, and χ. As we are interested in propagating solitons, we refer to t_0 and x_0 as the initial conditions, while the solitons themselves are characterized by χ, the soliton velocity in units of v_g, and ρ, the soliton amplitude. The initial condition t_0 defines the soliton's absolute phase, and is only important for problems dealing with multiple solitons, which we do not consider here. Parameter x_0 is unimportant, provided $|x_0|\gg0$, as we only consider perturbations to a uniform grating which begin near the origin. If the gap soliton is initially sufficiently far from the perturbation, the precise initial position does not matter and $|x_0|$ may be taken to be $-\infty$ for convenience.

In the presence of perturbations analytic soliton solutions do not usually exist. However, if the perturbations are small then we can make the EPP assumption that we can always describe the field as a gap soliton. Thus in the EPP approach we are interested in the time evolution of ρ and χ, as these uniquely define the gap soliton given the initial conditions x_0 and t_0. Our aim is thus to derive evolution equations for ρ and χ. This was done previously for a different class of perturbations [18], and so only the salient points are explicitly treated here. The EPP is derived by considering a small set of moments of the field which in the absence of perturbations completely characterize the gap soliton. The moments, which are analogous to those used in Ref. [14], are given below, where they are defined ($\equiv$) and then evaluated for a gap soliton ($=$). They are the energy Q,

$$Q\equiv\int_{-\infty}^{+\infty}(|f_+|^2+|f_-|^2)dx=\frac{2\rho\alpha^2}{\Gamma_x}; \tag{7}$$

the average position $\overline{x}$,

$$\overline{x}\equiv\frac{1}{Q}\int_{-\infty}^{+\infty}x(|f_+|^2+|f_-|^2)dx=x_0+\chi t; \tag{8}$$

and the momentum $\mathcal{P}$,

$$\mathcal{P}\equiv-i\int_{-\infty}^{+\infty}(f_+^*\partial_x f_++f_-^*\partial_x f_-)dx =\frac{2\kappa\chi\gamma}{\Gamma_x}\alpha^2\sin\rho+\frac{4\kappa\Gamma_s\chi\gamma^3}{\Gamma_x^2}\alpha^4(\sin\rho-\rho\cos\rho). \tag{9}$$

Both Q and $\mathcal{P}$ are conserved quantities of the unperturbed equations [21,22]. They have the property that for a single gap soliton, knowledge of these moments allows one to reconstruct it up to a constant phase factor.

Using the coupled mode equations [Eqs. (1)] the time derivatives of moments (7)–(9) can be calculated and are given in full in Ref. [18]. Here we only give the most relevant:

$$\frac{dQ}{dt}=0, \tag{10a}$$

$$\frac{d\mathcal{P}}{dt}=\int_{-\infty}^{+\infty}\left[|f_+|^2\frac{\partial V_{11}}{\partial x}+|f_-|^2\frac{\partial V_{22}}{\partial x}+2\Re\left(f_+ f_-^*\frac{\partial V_{21}}{\partial x}\right)\right]dx. \tag{10b}$$

Equation (10a) expresses energy conservation, while Eq. (10b) expresses the effect of the perturbation on the gap soliton. Equations (10) are exact; however, to evaluate the integrals we must know the field at all times, which involves solving the full NLCME. Instead, as mentioned, we assume the field always remains a gap soliton. Further simplifications can be made since $dQ/dt=0$, we can express $\rho(t)$ in terms of $\chi(t)$ and the initial energy Q_0 as

$$\rho(t)=\frac{Q_0\Gamma_x}{2\alpha(\chi(t))^2}, \tag{11}$$

leading to the final EPP set of equations:

$$\frac{d\overline{x}}{dt}=\chi, \tag{12a}$$

$$\frac{d\mathcal{P}}{dt}=F(\overline{x}), \tag{12b}$$

$$\mathcal{P}=\mathcal{P}(\chi). \tag{12c}$$

Here F is the ''force'' on a gap soliton found by evaluating the integrals in Eq. (10b). Note that our method explicitly calculates $\overline{x}$ rather than inferring it from the values of χ and ρ. This is done for clarity since in general the force on the gap soliton depends on its position. Henceforth, when we refer to solving the EPP equations we mean solving Eqs. (12). Note that the perturbation manifests itself through the force F. Thus, whenever analyzing a nonuniform grating using the EPP, the first step is always to evaluate the integral in Eq. (10b) to find the EPP force. As expected, the EPP force depends only on the gradient of the perturbation matrix, since when V is a constant Hermitian matrix, Eqs. (1) are identical to the NLCME's. Having derived the EPP we next discuss some general properties of the EPP before presenting some applications.

Here we are concerned with gap solitons propagating in nonuniform gratings of infinite extent. It is thus useful to reduce the parameter space as much as possible. For a uniform grating, one can rescale the NLCME's, resulting in $\kappa=1$ [8]. Similarly, one can set $\Gamma_s'=\Gamma_s/\Gamma_x$ and $\Gamma_x=1$, without loss of generality. For a nonuniform grating this rescaling results in $\kappa(x)=1$ at a single point which may be chosen arbitrarily. We can thus restrict ourselves to gratings for which $\kappa(x)\to 1$ and $\Gamma_x(x)\to 1$ as $x\to-\infty$. In fact, for the gratings we consider, $\kappa(x)=1$ if $x<-a$, where typically a is order unity. We similarly introduce a dimensionless length by $x\to x\kappa(-\infty)$. With these normalizations all quantities, including the fields in Eqs. (1), are dimensionless.

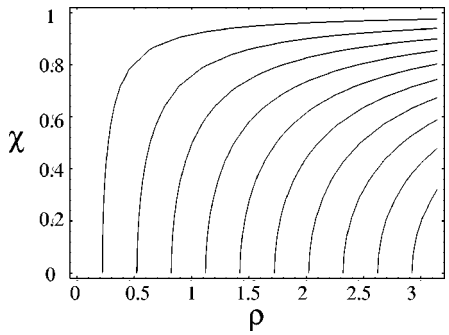

FIG. 1. Contour plot of constant energy as a function of ρ and χ.

General properties of the EPP

Equation (7) shows that the energy Q of a gap soliton is a function of both χ and ρ. Since in the EPP this energy is assumed to be conserved, $\chi(t)$ and $\rho(t)$ are constrained to move on contours of equal energy in the (ρ,χ) plane. These contours are shown in Fig. 1, and their analytic form is given in Eq. (11). Note that each contour has a maximum velocity χ_m which is reached when $\rho=\pi$. Inverting Eq. (7) when $\rho=\pi$ gives

$$\chi_m=\sqrt{\frac{4\pi-\Gamma_s Q_0-2\Gamma_x Q_0}{4\pi+\Gamma_s Q_0-2\Gamma_x Q_0}}, \tag{13}$$

where Q_0 is the initial energy of the gap soliton. Equation (13) shows that, in the EPP approximation, the smaller the initial energy of a gap soliton, the higher the maximum velocity it can attain. If our numerical simulations show that an initial gap soliton has accelerated past χ_m then either it has shed energy or the field has ceased to be a gap soliton. In either case the EPP is not valid. This arises in Sec. III B, and is discussed in more detail there. In the other cases we considered, the velocity of the gap soliton does not approach χ_m, and our EPP remains valid.

In the low velocity limit of the EPP ($\chi\ll 1$) we can approximate Eq. (12c) by

$$\mathcal{P}=\frac{16\kappa\Gamma_s}{9\Gamma_x^2}(\sin\rho-\rho\cos(\rho))\,\chi\equiv m\chi, \tag{14}$$

where m does not depend on velocity, and can be considered to be the ''mass'' of the soliton in analogy with Newtonian mechanics. In this low velocity limit our EPP equations are then formally identical to Newton's equations. If in this limit the force F depends only on position, then a potential $U(x)$ can be defined as [18]

$$U(\overline{x})=-\int_{-\infty}^{x}F(x')dx'. \tag{15}$$

The EPP equations can then be solved exactly, giving

$$\chi(\overline{x})^2-\chi(x_0)^2=\frac{2}{m}(U(x_0)-U(x)), \tag{16}$$

where x_0 is the initial position of the gap soliton.

Given a maximum height U of a potential, then Eq. (16) implies that gap solitons with velocities less than

$$\chi_u = \sqrt{\frac{2U}{m}} \tag{17}$$

are reflected. Note that for a sufficiently large height, Eq. (17) predicts a velocity for which the potential approximation is no longer valid. Thus care must be taken to ensure that the results are not used outside the velocity regime for which the potential approximation is valid.

The class of nonuniform gratings is too large to test the EPP on every different type. Instead we restrict ourselves to a few generic grating types which can be fabricated, and which let us develop a general understanding. A further restriction is that we only consider gratings for which the integral for the EPP force [Eq. (10b)] can be evaluated exactly. In this case the EPP equations reduce to two ordinary differential equations which can be efficiently solved numerically. Otherwise, finding numerical solutions to the EPP equations is as computationally intensive as the full numerical simulations. The simplest class of gratings that fulfill these requirements are gratings whose parameters are piecewise linear functions of position. Such gratings are considered in Sec. III.

III. PROPAGATION ALONG A RAMP

A. A κ ramp

In the perturbation considered here, the grating strength varies linearly with position for $x>0$, but the Bragg frequency is constant. Hence κ is given by

$$\kappa(x) = \begin{cases} \kappa_0, & x<0 \\ \kappa_0 + \Delta_\kappa x, & x>0, \end{cases} \tag{18}$$

where $\Delta_\kappa > 0$. We take the grating to be infinitely long with the strength increasing without bounds as $x \to \infty$. Since, as we show below, any such incident soliton is ultimately reflected, the idealization of the grating strength growing without bound is not essential. However, the time spent in the perturbed region depends on the gap soliton's parameters. Such a grating could thus act as a nonlinear mirror with the time delay varying nonlinearly with the incident energy.

For the grating described in Eq. (18), the perturbation matrix V vanishes for $x<0$. For $x>0$ we have

$$V = \begin{pmatrix} 0 & \Delta_\kappa x \\ \Delta_\kappa x & 0 \end{pmatrix}. \tag{19}$$

Substituting Eq. (19) into Eq. (10b) we obtain [23]

$$\frac{d\mathcal{P}}{dt} = -\frac{\Delta_\kappa \alpha^2}{\gamma}\frac{\sin\rho}{\Gamma_x} \times \left(1 + \frac{\sinh(2\gamma\kappa_0 \sin[\rho]\overline{x})}{\cosh(2\gamma\kappa_0 \sin[\rho]\overline{x}) + \cos\rho}\right), \tag{20}$$

where $\overline{x}$ is the gap soliton location [Eq. (8)]. Note that in Eq. (20) only κ_0 and not $\kappa(x)$ appears in the argument of the hyperbolic functions. This is so since for our ansatz we took the gap soliton solutions for a uniform grating of strength κ_0. When Δ_κ is sufficiently small, $\kappa(x)$ does not vary considerably over the width of a gap soliton, and thus we can replace κ_0 by $\kappa(\overline{x})$ in Eq. (20). This results in a slight improvement in the EPP accuracy.

For $\overline{x} \gg 0$ the right hand side of Eq. (20) approaches a constant. When $\rho \leqslant \pi/2$ the sign of $d\mathcal{P}/dt$ is always negative, implying that the soliton is repelled by the ramp, as expected. In contrast, when $\rho > \pi/2$ the force on the gap soliton is positive for $\overline{x} < x_0$, where

$$x_0 = \frac{-1}{2\gamma\kappa\sin\rho}\cosh^{-1}\left(\frac{-(1+\cos^2\rho)}{2\cos\rho}\right), \tag{21}$$

at which point $d\mathcal{P}/dt$ changes sign and the gap soliton is repelled thereafter. Thus in the EPP picture, at least, all solitons are reflected by the ramp. We note that previously we found that, for an abrupt interface, stationary solutions only exist for $\rho > \pi/2$, and we were able to find exact solutions to the NLCME's [18]. However, unlike the abrupt interface, we have been unable to find exact analytic expressions for stationary solutions in this case.

Recall that for low velocities $\mathcal{P} \propto \chi$ and that the EPP equations are then formally identical to Newton's equations of motion. For the force in Eq. (20), the low velocity approximations leads to the potential

$$U(\overline{x}) = \alpha^2 \frac{\Delta_\kappa}{2\Gamma_x}[4\kappa \sin[\rho]\overline{x} + \ln(1 + 2e^{-2\kappa \sin[\rho]\overline{x}}\cos\rho + e^{-4\kappa \sin[\rho]\overline{x}})]. \tag{22}$$

In this limit the velocity χ of the gap soliton is given by Eq. (16). For large $\overline{x}$ we can approximate the potential in Eq. (22) by

$$U(\overline{x}) \approx \alpha^2 \frac{\Delta_\kappa}{\Gamma_x} 2\kappa \sin[\rho]\overline{x}. \tag{23}$$

Note that when $\rho > \pi/2$ the potential has a minimum at a position given by Eq. (21), suggesting that stationary solitons might exist and be stable.

We now have two approximations to the trajectories: the exact EPP trajectory obtained by solving Eq. (20) numerically; and a low velocity approximation, following from the potential in Eq. (22). Since our numerical simulations show that all incident gap solitons are reflected, the main feature of the trajectory is the position of the turning point. It describes how far the gap soliton ventures into the perturbed region, and gives an indication of the time it spends there. Equation (23) leads to the approximation for the turning point x_t,

$$x_t \approx \frac{\Gamma_x m \chi^2}{2\alpha^2 \kappa \Delta_\kappa \sin\rho}, \tag{24}$$

where m was defined in Eq. (14). Figure 2 shows the turning point versus velocity, for all different methods. On this scale they are indistinguishable, indicating that the exact EPP is in

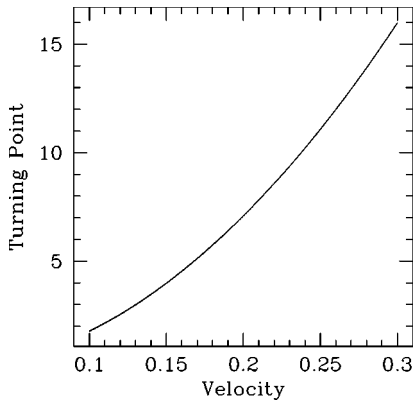

FIG. 2. Normalized turning point vs the incident velocity in units of v_g for a gap soliton with $\rho=2$, and for a grating with $\kappa=1$ and $\Delta_\kappa=0.01$. The normalized position $\tilde{x}=x\kappa$ is dimensionless.

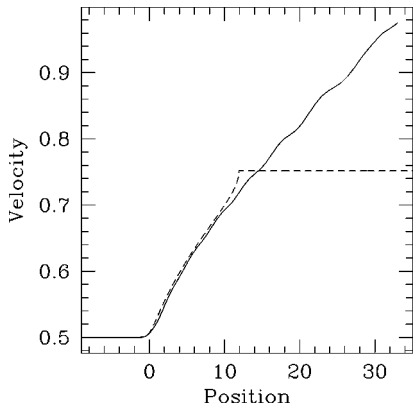

FIG. 3. Trajectory showing velocity (in units of v_g) vs the dimensionless position (normalized in terms of κ) for a gap soliton. The solid line gives the exact results and the dashed line the EPP trajectory. The grating has $\kappa=1$ and $\Delta_\delta=0.05$. Initially the gap soliton has $\rho=2$ and $\chi=0.5$.

good agreement with the numerical result. Furthermore, the low velocity approximation to the EPP holds for the velocities considered in Fig. 2.

In the numerical simulations of NLCME's with a κ ramp, we found that upon reflection the gap soliton would begin to oscillate [24]. These oscillations seem to be a generic response of gap solitons [25] (and nonintegrable systems [26]) to perturbation and in some cases leads to the destruction of the soliton. As discussed in Ref. [18], the EPP assumes the gap soliton has no internal degrees of freedom, and hence cannot describe the gap soliton oscillations.

B. A δ ramp

The other type of grating we consider is one where the Bragg frequency varies linearly for $x>0$. Thus the perturbation matrix V vanishes for $x<0$, whereas, for $x>0$,

$$V=\begin{pmatrix}\Delta_\delta x & 0\\ 0 & \Delta_\delta x\end{pmatrix}. \tag{25}$$

Solving the EPP integrals leads to

$$\frac{d\mathcal{P}}{dt}=\frac{2\alpha^2\Delta_\delta}{\Gamma_x}\left[\frac{\rho}{2}-\tan^{-1}\left(\tanh(-\gamma\kappa\sin[\rho]\overline{x})\tan\frac{\rho}{2}\right)\right]. \tag{26}$$

Note that the EPP force never changes sign, and approaches a constant for $\overline{x}\gg 0$. This implies that for $\Delta_\delta<0$ gap solitons are always repelled by the barrier, while for $\Delta_\delta>0$ the gap soliton's velocity increases.

When $\Delta_\delta<0$ the gap soliton moves deeper into the band gap as it propagates toward $+\infty$. This causes it to be reflected by the grating. As for the case of a κ ramp, the EPP accurately predicts the position of the turning point. We note that, in the low velocity limit, potential Eq. (15) for this EPP force is valid. However, we cannot find a closed-form analytic expression for the potential. Thus finding the trajectory of the gap soliton using the potential is computationally as time consuming as solving the EPP equations exactly.

When $\Delta_\delta>0$, the gap soliton moves away from the center of the band gap as it propagates through the grating. Eventually its original center frequency is outside the band gap. As the gap soliton continues to propagate, the group velocity of its center frequency asymptotically approaches v_g. Now a NLSE soliton propagating through a dispersion decreasing fiber is compressed [27]. In the limit when the gap soliton is outside the band gap, the coupled mode equations reduce to the NLSE with varying dispersion [28], and thus we expect that an incident gap soliton is compressed as well. Numerical simulations confirm this, and show a compression ratio of nearly three for the gap soliton width. A pulse compression scheme of this type was recently discussed in Ref. [29].

Figure 3 shows a comparison between the EPP trajectory and the exact results for a gap soliton propagating down a ramp with $\Delta_\delta=0.05$. Note that initially the EPP trajectory is accurate, but fails at $x\approx 10$, with the EPP trajectory reaching a final velocity while the exact results suggest that the gap soliton continues to accelerate. The difference can be understood by recalling that earlier we showed that conservation of energy limits the maximum velocity χ_m a gap soliton may achieve according to the EPP [see Eq. (13) and Fig. 1]. The existence of a maximum velocity can be seen in Fig. 3, which shows the EPP trajectory levelling off after reaching χ_m.

The full numerical simulations in Fig. 3 show the field distribution reaching velocities exceeding χ_m. As discussed in Sec. II, this may occur in one of two ways: either the gap soliton sheds energy, allowing it to move to a different contour in Fig. 1, but remaining a gap soliton, or the field distribution ceases to be a gap soliton. In either case the EPP fails. From numerical simulations it appears that the gap soliton behavior is a combination of the two, initially shedding energy while retaining its shape but quickly breaking up into multiple pulses. This is illustrated in Fig. 4, which shows the field distribution after propagation for an initial gap soliton with $\rho=1$ and $\chi=0.5$. Note also the long energy tail which has been shed by the gap soliton. Thus our EPP accurately predicts the gap soliton's trajectory if $\Delta_\delta<0$, and is initially accurate if $\Delta_\delta>0$. In the latter case the gap soliton eventually breaks up, and thus the failure of our method is not surprising.

One can also consider gratings that have both κ and δ ramps. Then the force felt by the EPP particle is the sum of the right hand side of Eqs. (20) and (26). For such gratings

the EPP describes the motion of the gap soliton with an accuracy similar to the two separate cases considered above. As no new features are introduced, we do not present results, but instead turn to a different type of grating.

IV. PROPAGATION THROUGH LOCALIZED PERTURBATIONS

By combining two ramps we can make a grating which has a localized defect given by

$$V_{ij}(x)=\begin{cases}0, & |x|>a\\ (x+a)\Delta_{ij}, & -a\leqslant x<0\\ (a-x)\Delta_{ij}, & 0\leqslant x<a,\end{cases} \tag{27}$$

where $2a$ is the width of the perturbation, and the strength is given by the Hermitian matrix Δ_{ij}. The off-diagonal entries $\Delta_{12}=\Delta_{21}^{*}$ describe changes in the strength of the grating, while the diagonal elements describe a shift in the Bragg condition. Henceforth we denote the off-diagonal elements by Δ_{κ}, and the diagonal elements by Δ_{δ}. Note that defect (27) is symmetric, though this is not essential. We chose this form since it is the simplest localized defect, and since the EPP integrals can be solved exactly. We concentrate on this as we expect that general types of behavior of gap solitons in the presence of more general defects can be captured by this model.

For defect (27), $\mathcal{P}$ evolves according to

$$\frac{d\mathcal{P}}{dt}=\Delta_{\kappa}f_1+\Delta_{\delta}f_2, \tag{28}$$

where

$$f_1=-\frac{\alpha^2\sin\rho}{\Gamma_x\gamma}\left[\frac{2\sinh(-2\gamma\kappa\sin[\rho]\overline{x})}{\cos\rho+\cosh(-2\gamma\kappa\sin[\rho]\overline{x})}-\frac{\sinh(-2\gamma\kappa\sin[\rho](\overline{x}+a))}{\cos\rho+\cosh(-2\gamma\kappa\sin[\rho](\overline{x}+a))}-\frac{\sinh(-2\gamma\kappa\sin[\rho](a-\overline{x}))}{\cos\rho+\cosh(-2\gamma\kappa\sin[\rho](a-\overline{x}))}\right] \tag{29a}$$

and

$$f_2=-\frac{2\alpha^2}{\Gamma_x}\left[2\tan^{-1}\left(\tanh(-\gamma\kappa\sin[\rho]\overline{x})\tan\left(\frac{\rho}{2}\right)\right)-\tan^{-1}\left(\tanh(\gamma\kappa\sin[\rho](a-\overline{x}))\tan\left(\frac{\rho}{2}\right)\right)\right.$$
$$\left.-\tan^{-1}\left(\tanh(-\gamma\kappa\sin[\rho](a+\overline{x}))\tan\left(\frac{\rho}{2}\right)\right)\right]. \tag{29b}$$

Since f_2 represents two δ ramps, Eq. (29b) is very similar to the right hand side of Eq. (26). Similarly, f_1 represents two κ ramps, and resembles the right hand side of Eq. (20).

To illustrate the accuracy of the EPP for perturbation (27), we show the case where $\Delta_{\kappa}=-0.02$, $\Delta_{\delta}=-0.04$, $\kappa=1$, and $a=5$. Figure 5 shows the exact and approximate trajectories for a gap soliton with $\rho=1.5$ and a varying initial velocity. The two dashed vertical lines show the perturbed region. In all cases the agreement between the EPP and the exact results is very good, the only difference being a slight oscillation in the exact results after the gap soliton has traveled through the perturbation.

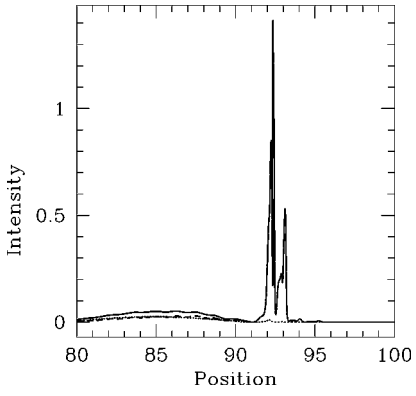

FIG. 4. Field distribution as a function of position for a gap soliton initially with $\rho=1$ and $\chi=0.5$ after propagation along a ramp with $\Delta_{\delta}=0.05$. Note that the gap soliton has broken up into two pulses along with a long radiation tail. The dashed line shows $|f_{+}|^2$, the dotted line $|f_{-}|^2$, and the solid line the total intensity $|f_{+}|^2+|f_{-}|^2$.

The trajectories in Fig. 5 suggest that the gap soliton experiences a potential barrier, since it slows down as it enters the perturbed region. As discussed, we can define a potential for the EPP force, and, as expected from Fig. 5, the potential now consists of a single peak near the origin. Since for a δ ramp an analytic expression for the potential cannot be found, f_2 cannot be integrated, unlike f_1. Calculating the potential numerically, we find that the peak height of the potential for Fig. 5 is 0.226 which, using Eq. (22), implies that gap solitons with a velocity less than 0.394 are reflected. Numerical solutions of the EPP give a maximum reflected velocity of 0.355, which is identical to the value found from full simulations of the NLCME. The small discrepancy is to be expected since the condition $|v|\ll 1$ is not satisfied everywhere.

It is well known how a point defect in the grating introduces a resonant state within the band gap, leading to zero reflection at the resonant frequency [30]. For gratings with a localized defect the same holds true. In Fig. 6 we show the reflection spectrum for a grating with parameters as in Fig. 5.

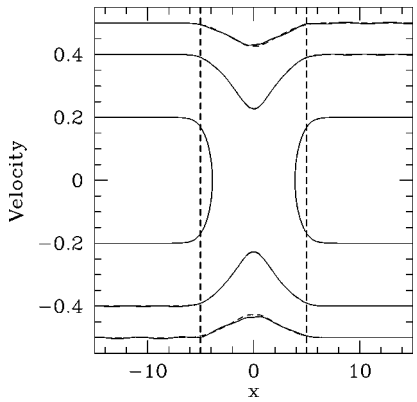

FIG. 5. Trajectory showing velocity (in units of v_g) vs the position of a gap soliton with $\rho=1.5$. The solid line gives the exact results, and the dashed line the EPP trajectory. The two dashed vertical lines indicate the perturbed region.

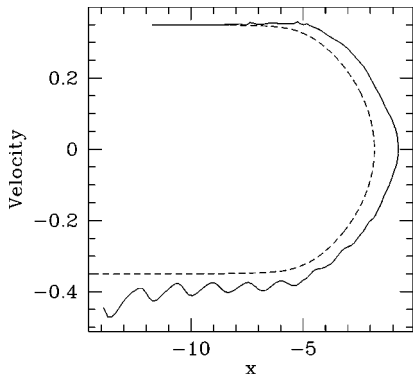

FIG. 7. Phase portrait showing velocity (in units of v_g) vs normalized position for a gap soliton whose center frequency coincides with the frequency of the resonant zero of the grating. The solid line shows the exact result, while the dashed line shows the EPP approach.

The effect of the resonant state is indicated by the dashed portion of the curve; it clearly shows a reflection zero within the band gap of the grating. The effect of this localized state can also be seen in the propagation of gap solitons with a center frequency near the resonance. Figure 7 shows the phase portrait for a gap soliton with $\rho=2.733\,13$ and $\chi=0.35$. These parameters ensure that the center frequency of the gap soliton coincides with the resonance. Compared to previous results, we see a marked difference between exact and EPP results: the gap soliton is reflected with a different velocity, and undergoes considerable oscillations. Most of these differences are due to the increased radiation losses. Due to the resonant zero the low intensity wings can propagate through the grating instead of being reflected back toward the center of the gap soliton. This interaction with the defect state causes the soliton to move off the EPP contour, and our approximation thus breaks down.

So far we have concentrated on the case when Δ_κ and Δ_δ are negative. If Δ_κ and Δ_δ are both positive, the potential hill becomes a potential well. Gap solitons thus speed up as they enter the perturbed region. The accuracy of the EPP in this region is similar to the case of a potential hill. The presence of a potential well allows for trapped solitons which oscillate around the center of the grating, as well as stable stationary solutions centered at $x=0$. Figure 8 shows the phase portrait for a gap soliton with $\rho=1.5$ trapped inside a well with $\Delta_\kappa=0.02$, $\Delta_\delta=0.04$, and $a=5$. The solid line shows the exact trajectory, while the dashed line shows the EPP trajectory. Note that the EPP particle travels further up the side of the wall compared to the exact results. Although both the EPP particle and the gap soliton started at $\bar{x}=0$ with $\chi=0.3$, the gap soliton never regains its initial velocity, instead settling down to a smaller limit cycle with a maximum velocity of about 0.278.

Earlier, we stated that linear barriers as discussed here are typical of the more general class of localized defects, and thus the understanding of such defects would lead to a more general understanding of gap soliton propagation. As an example, we examined gap soliton propagation through a Gaussian defect given by

$$V_{ij}(x)=\Delta_{ij}ae^{-(x^2/a^2)4\ln 2}. \tag{30}$$

This defect has the same peak strength and full width at half maximum as the linear barrier given by Eq. (27). In Fig. 9 the solid line shows gap soliton trajectories for a Gaussian barrier with $\Delta_\kappa=-0.02$, $\Delta_\delta=-0.04$, and $a=5$. The dashed lines show the trajectories for the linear barrier with the same parameters as was used in Fig. 5. The vertical lines again indicate the position of the perturbed region.

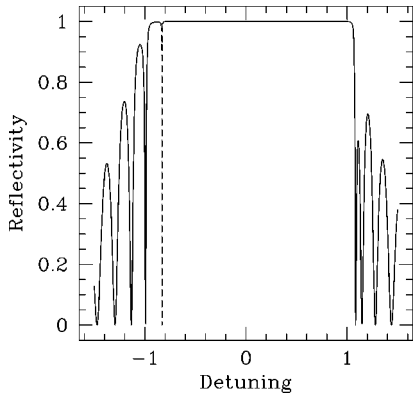

FIG. 6. Reflection vs detuning in units of κ for a grating with a localized defect, with parameters given in the text. The defect leads to a zero reflection, as indicated by the dashed line.

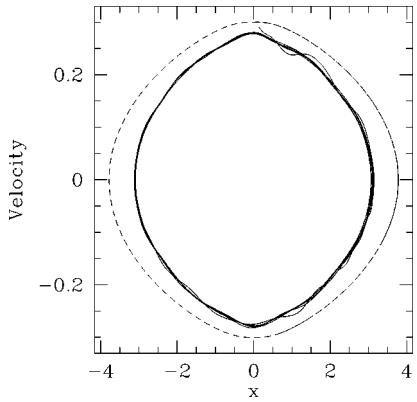

FIG. 8. Trajectory showing velocity (in units of v_g) vs normalized position for a gap soliton with $\rho=1.5$. The solid line gives the exact results, and the dashed line the EPP trajectory.

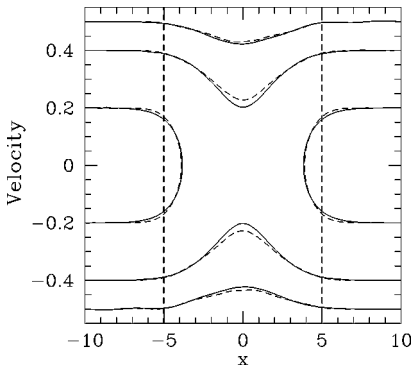

FIG. 9. Trajectories showing velocity (in units of v_g) vs normalized position for a gap soliton with $\rho=1.5$, in the presence of a Gaussian barrier. The solid line gives the exact results, and the dashed line the results for a linear barrier.

Although for the Gaussian barrier we are not able to evaluate the integrals in the EPP equations of motion analytically, Fig. 9 suggests that the Gaussian barrier behaves qualitatively the same as a linear barrier. Extending this, we suggest that for a sufficiently smooth barrier the only quantities of importance are the peak height and barrier width. Gap solitons thus behave qualitatively the same when perturbed by a wide range of barriers. Furthermore, we can approximate all such barriers by a linear barrier and use the EPP formalism to understand the results in these cases.

V. GRADUAL INTERFACES

Earlier [18], we concentrated on abrupt interfaces between two uniform gratings. As a last example we consider two semi-infinite uniform gratings, with the parameters changing continuously between $x=-a$ and $x=a$. In line with the notation used in Ref. [18], we define

$$\kappa=\begin{cases}\kappa_l, & x<-a\\ \kappa_l+\dfrac{\kappa_r-\kappa_l}{2a}(x+a), & -a\leqslant x\leqslant a\\ \kappa_r, & x>a.\end{cases} \tag{31}$$

Hence, for gap solitons whose center position $\bar{x}$ satisfies $\bar{x}<0$, we have the perturbation matrix

$$V_{12}(x)=V_{21}(x)=\begin{cases}0, & x<-a\\ \dfrac{\kappa_r-\kappa_l}{2a}(x+a), & -a\leqslant x\leqslant a\\ \kappa_r-\kappa_l, & x>a.\end{cases} \tag{32}$$

Similarly for solitons lying to the right of the origin, we have

$$V_{12}(x)=V_{21}(x)=\begin{cases}\kappa_l-\kappa_r, & x<-a\\ \dfrac{\kappa_r-\kappa_l}{2a}(x-a), & -a\leqslant x\leqslant a\\ 0, & x>a.\end{cases} \tag{33}$$

In both cases $V_{11}=V_{22}=0$.

Substituting Eq. (32) into Eq. (10b), we obtain

$$\frac{d\mathcal{P}}{dt}=\frac{\kappa_l-\kappa_r}{2a}\frac{\alpha^2\sin\rho}{\gamma\Gamma_x}\times\left[\frac{\sinh(2\gamma\kappa_l\sin[\rho](a-\bar{x}))}{\cos\rho+\cosh(2\gamma\kappa_l\sin[\rho](a-\bar{x}))}+\frac{\sinh(2\gamma\kappa_l\sin[\rho](a+\bar{x}))}{\cos\rho+\cosh(2\gamma\kappa_l\sin[\rho](a+\bar{x}))}\right]. \tag{34}$$

When $\bar{x}>0$ we obtain a similar expression but with κ_l replaced by κ_r. Taking the limit of the right hand side of Eq. (34) as $a\to 0$, we find an expression that is identical to Eq. (32) in Ref. [18] for $d\mathcal{P}/dt$ for an abrupt interface. Since we know that the EPP gives accurate results for an abrupt interface, our gradual model is expected to be accurate for small a. Also in the limit that $\kappa_r\gg\kappa_l$ and $a\gg 1$, the grating appears nearly identical to the κ ramp discussed above, as in this limit the gap soliton only ''sees'' the ramp and not the uniform grating behind it.

When $\chi\to 0$, Eq. (34) does not depend on χ, and Eq. (15) is then valid. The resulting potential is

$$U_l(\bar{x})=\frac{\kappa_r-\kappa_l}{2a}\frac{\alpha^2}{2\kappa_l\Gamma_x}\left[\ln\left(\frac{\cos\rho+\cosh(2\kappa_l\sin[\delta](a+\bar{x}))}{\cos\rho+\cosh(2\kappa_l\sin[\delta](a-\bar{x}))}\right)+4\kappa_l a\sin\rho\right], \tag{35a}$$

which is valid for $\bar{x}<0$. For $\bar{x}>0$ we have

$$U_r(\bar{x})=\frac{\kappa_r-\kappa_l}{2a}\frac{\alpha^2}{2\kappa_r\Gamma_x}\left[\ln\left(\frac{\cos\rho+\cosh(2\kappa_r\sin[\delta](a+\bar{x}))}{\cos\rho+\cosh(2\kappa_r\sin[\delta](a-\bar{x}))}\right)-4\kappa_r a\sin\rho\right]+C. \tag{35b}$$

Thus the asymptotic height H of this potential is

$$H=2\alpha^2\frac{\kappa_r-\kappa_l}{\Gamma_x}\sin\rho, \tag{36}$$

which is independent of a, and is identical to the expression for an abrupt interface (see Fig. 3 in Ref. [18]). Thus the final velocity of the gap soliton is independent of whether the grating changes linearly or discontinuously, which is broadly

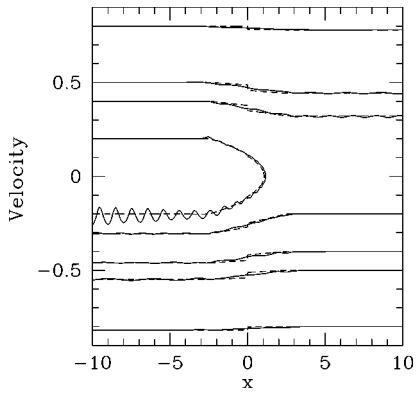

FIG. 10. Trajectories showing velocity (in units of v_g) vs normalized position for a gap soliton with $\rho=2$, in the presence of a gradual interface with $a=2.5$, $\kappa_l=1$, and $\kappa_r=1.1$. The solid line gives the exact results, and the dashed line the results for a linear barrier.

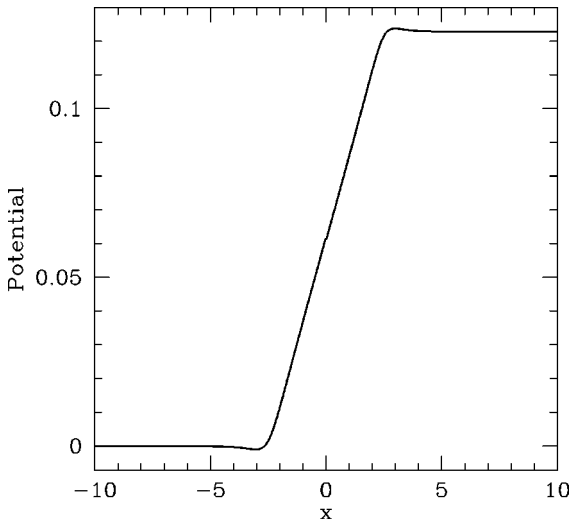

FIG. 11. Graph of the potential for a gradual interface. Here $\kappa_l=1$, $\kappa_r=1.1$, and $a=2.5$.

consistent with Sec. IV. All that is important in determining the final velocity, assuming that the gap soliton is not reflected, is the difference in parameters of the two uniform gratings.

In Fig. 10 we show a variety of trajectories with $\rho=2$, $\kappa_l=1$, and $\kappa_r=1.1$, with $a=2.5$. It should be compared with Fig. 5 of Ref. [18], which shows similar trajectories for an abrupt interface. The key difference is the trajectory for $\chi=0.2$, which shows significant oscillations after reflection. The other trajectories at the gradual interface show fewer oscillations than at the abrupt interface. The reasons for the increased oscillations in the reflected trajectory are not understood at present.

Figure 11 shows the associated potential [Eq. (35)]. The asymptotic height H of the gradual interface potential is 0.121 24, corresponding to a maximum reflected velocity of 0.237. Numerical integration of the EPP equations show that gap solitons with a velocity of less than 0.238 are reflected, while numerical simulations give 0.235. For the corresponding abrupt interface gap, solitons with a velocity of less at 0.242 are reflected, which is somewhat higher than for the gradual interface. This discrepancy can be understood from the graphs of the two potentials (Figs. 11 and 3 in Ref. [18]). For the gradual interface the maximum height of the potential is roughly the same as the asymptotic height. In contrast, for the abrupt case the maximum height is higher than the asymptotic height. Similarly the minimum of the potential for the abrupt case is less than for the gradual case. This difference also allows stable stationary solutions to exist for the abrupt interface but not for the gradual interface.

VI. CONCLUSIONS

The EPP described in Ref. [18] and extended here is a powerful tool for understanding gap soliton propagation through nonuniform gratings. In the low velocity limit, the EPP equations reduce to that of a clasical particle moving in an external potential, determined by the nonuniformity. Although we have only examined a few highly idealized grating types, the insights gained should be applicable to more general geometries. We showed that for a localized defect there is no significant difference between a Gaussian defect and a linear one, for which exact results are available. This suggests that the rough gap solitons behavior depends only on the general features of the perturbation and not the details. This is further confirmed by the results in Sec. V for an abrupt interface, which are nearly identical to those derived in our earlier paper for an abrupt interface.

We should mention that the manipulation of gap solitons by propagation through a nonuniform grating is very attractive. An example is the gap soliton compression in a grating with a δ ramp, which is similar to soliton compression in a dispersion-decreasing fiber (see Sec. III B). Note that the required grating is of a standard type, and can be written in a standard photosensitive fiber [29]. In contrast, dispersion-decreasing fiber is highly specialized. Moreover, because of the strong coupling between the electric field and the grating at frequencies around the Bragg resonance, the magnitude of the perturbation in a grating can be made much larger than the perturbation in untreated fiber.

A feature of our full simulations is that in many cases the perturbed gap soliton starts oscillating. It is well known theoretically that oscillation modes of gap solitons exist [24]; however, these have not yet been observed. Reflection off a perturbation would appear to be a possible way to set up such modes experimentally, as the gratings required can easily be fabricated. Furthermore in some cases these oscillations grow and eventually destroy the soliton in line with recent predictions [25]. This instability does not appear in our model, as we have assumed that the gap soliton has no internal degrees of motion.

Throughout this work we have assumed that the grating is lossless. This is not a necessary condition for the EPP to work but rather it has been shown that the EPP can be successfully applied to gratings with gain and/or loss, and hence we did not consider it here. Similarly we have not examined periodic perturbations, since in that case it has been shown that a superenvelope approach to the coupled mode equations is very successful, and allows analytic solutions to be found [31,32].

[1] D. Taverner, N. G. R. Broderick, D. J. Richardson, R. I. Laming, and M. Ibsen, Opt. Lett. **23**, 328 (1998).
[2] D. Taverner, N. G. R. Broderick, D. J. Richardson, M. Ibsen, and R. I. Laming, Opt. Lett. **23**, 259 (1998).
[3] B. J. Eggleton, R. E. Slusher, C. M. de Sterke, P. A. Krug, and J. E. Sipe, Phys. Rev. Lett. **76**, 1627 (1996).
[4] B. J. Eggleton, C. M. de Sterke, and R. E. Slusher, J. Opt. Soc. Am. B **14**, 2980 (1997).
[5] B. J. Eggleton, C. M. de Sterke, A. B. Aceves, J. E. Sipe, T. A. Strasser, and R. E. Slusher, Opt. Commun. **149**, 267 (1998).
[6] M. Durkin, M. Ibsen, M. J. Cole, and R. I. Laming, Electron. Lett. **33**, 1891 (1997).
[7] H. G. Winful, J. H. Marburger, and E. Garmire, Appl. Phys. Lett. **35**, 379 (1979).
[8] C. M. de Sterke and J. E. Sipe, in *Progress in Optics*, edited by E. Wolf (North-Holland, Amsterdam, 1994), Vol. XXXIII, Chap. III, pp. 203–260.
[9] J. E. Sipe, L. Poladian, and C. M. de Sterke, J. Opt. Soc. Am. A **11**, 1307 (1994).
[10] Y. S. Kivshar, Phys. Rev. E **51**, 1613 (1995).
[11] A. B. Aceves and S. Wabnitz, Phys. Lett. A **141**, 37 (1989).
[12] D. N. Christodoulides and R. I. Joseph, Phys. Rev. Lett. **62**, 1746 (1989).
[13] J. Feng and F. K. Kneubühl, IEEE J. Quantum Electron. **29**, 590 (1993).
[14] A. B. Aceves, J. V. Moloney, and A. C. Newell, Phys. Rev. A **39**, 1809 (1989).
[15] V. E. Zakharov and A. B. Shabat, Sov. Phys. JETP **34**, 62 (1972).
[16] C. M. de Sterke and J. E. Sipe, Phys. Rev. A **43**, 2467 (1991).
[17] M. J. Steel and C. M. de Sterke, Phys. Rev. A **48**, 1625 (1993).
[18] N. Broderick and C. M. de Sterke, Phys. Rev. E **51**, 4978 (1995).
[19] A. D. Capobianco, C. De Angelis, A. Laureti Palma, and G. F. Nalesso, J. Opt. Soc. Am. B **14**, 1956 (1997).
[20] C. Conti, S. Trillo, and G. Assanto, Phys. Rev. E **57**, R1251 (1998).
[21] D. J. Kaup and A. C. Newell, Lett. Nuovo Cimento **20**, 325 (1977).
[22] E. A. Kuznetsov and A. V. Mikhailov, Theor. Math. Phys. **30**, 193 (1977).
[23] I. S. Gradshteyn and I. M. Ryzhik, in *Table of Integrals, Series and Products*, 5th ed., edited by A. Jeffrey (Academic, London, 1996).
[24] B. A. Malomed and R. S. Tasgal, Phys. Rev. E **49**, 5787 (1994).
[25] I. V. Barashenkov, D. E. Pelinovsky, and E. V. Zemlyanaya, Phys. Rev. Lett. **80**, 5117 (1998).
[26] Y. S. Kivshar, D. E. Pelinovsky, T. Cretegny, and M. Peyrard, Phys. Rev. Lett. **80**, 5032 (1998).
[27] S. V. Chernikov, E. M. Dianov, D. J. Richardson, and D. N. Payne, Opt. Lett. **18**, 476 (1993).
[28] C. M. de Sterke and J. E. Sipe, Phys. Rev. A **42**, 550 (1990).
[29] G. Lenz, B. J. Eggleton, and N. Litchinitser, J. Opt. Soc. Am. B **15**, 715 (1997).
[30] J. Canning and M. G. Sceats, Electron. Lett. **30**, 1344 (1994).
[31] N. G. R. Broderick and C. M. de Sterke, Phys. Rev. E **55**, 3634 (1997).
[32] N. G. R. Broderick, C. M. de Sterke, and B. J. Eggleton, Phys. Rev. E **52**, R5788 (1995).